Int J Adv Manuf Technol (2011) 57:49–60
DOI 10.1007/s00170-011-3262-1

ORIGINAL ARTICLE

The selection of milling parameters by the PSO-based neural network modeling method

Masoud Farahnakian · Mohammad Reza Razfar · Mahdi Moghri · Mohsen Asadnia

Received: 16 August 2010 / Accepted: 7 March 2011 / Published online: 6 April 2011

Abstract During the past decade, polymer nanocomposites have emerged relatively as a new and rapidly developing class of composite materials and attracted considerable investment in research and development worldwide. An increase in the desire for personalized products has led to the requirement of the direct machining of polymers for personalized products. In this work, the effect of cutting parameters (spindle speed and feed rate) and nanoclay (NC) content on machinability properties of polyamide-6/nanoclay (PA-6/NC) nanocomposites was studied by using high speed steel end mill. This paper also presents a novel approach for modeling cutting forces and surface roughness in milling PA-6/NC nanocomposite materials, by using particle swarm optimization-based neural network (PSONN) and the training capacity of PSONN is compared to that of the conventional neural network. In this regard, advantages of the statistical experimental algorithm technique, experimental measurements artificial neural network and particle swarm optimization algorithm, are exploited in an integrated manner. The results indicate that the nanoclay content on PA-6 significantly decreases the cutting forces, but does not have a considerable effect on surface roughness. Also the obtained results for modeling cutting forces and surface roughness have shown very good training capacity of the proposed PSONN algorithm in comparison to that of a conventional neural network.

Keyword Polyamide 6-nanoclay · Milling · Particle swarm optimization · Artificial neural network

M. Farahnakian · M. R. Razfar (✉)
Department of Mechanical Engineering,
Amirkabir University of Technology,
424, Hafez Ave,
Tehran, Iran
e-mail: razfar@aut.ac.ir

M. Moghri
Polymer Engineering Group, Islamic Azad University,
Kashan Branch,
Kashan, Iran

M. Asadnia
Faculty of Engineering, Iran University of Industries and Mines,
Tehran, Iran

1 Introduction

Recent researches on polymer-layered silicate nanocomposites have shown remarkable improvement of tensile modulus and tensile strength [1, 2]. The substantial improvements in mechanical, thermal, and physical properties of polymer-layered silicate nanocomposites have widened the use of these polymers in industry. In the late 1980s, the Toyota Motor Company commercialized a timing belt cover made from nylon-6/nanoclay (NC) composites for one of its car models demonstrating that thermoplastic nanocomposites are one of the most promising materials to use in domestic and industrial applications [3]. More recently, researchers Kojima et al. [4] and Kato et al. [5] showed that for nylon-6/MMT nanocomposites very small amounts of layered silicate loadings, approximately 5 wt.%, resulted in pronounced improvements of thermal and mechanical properties.

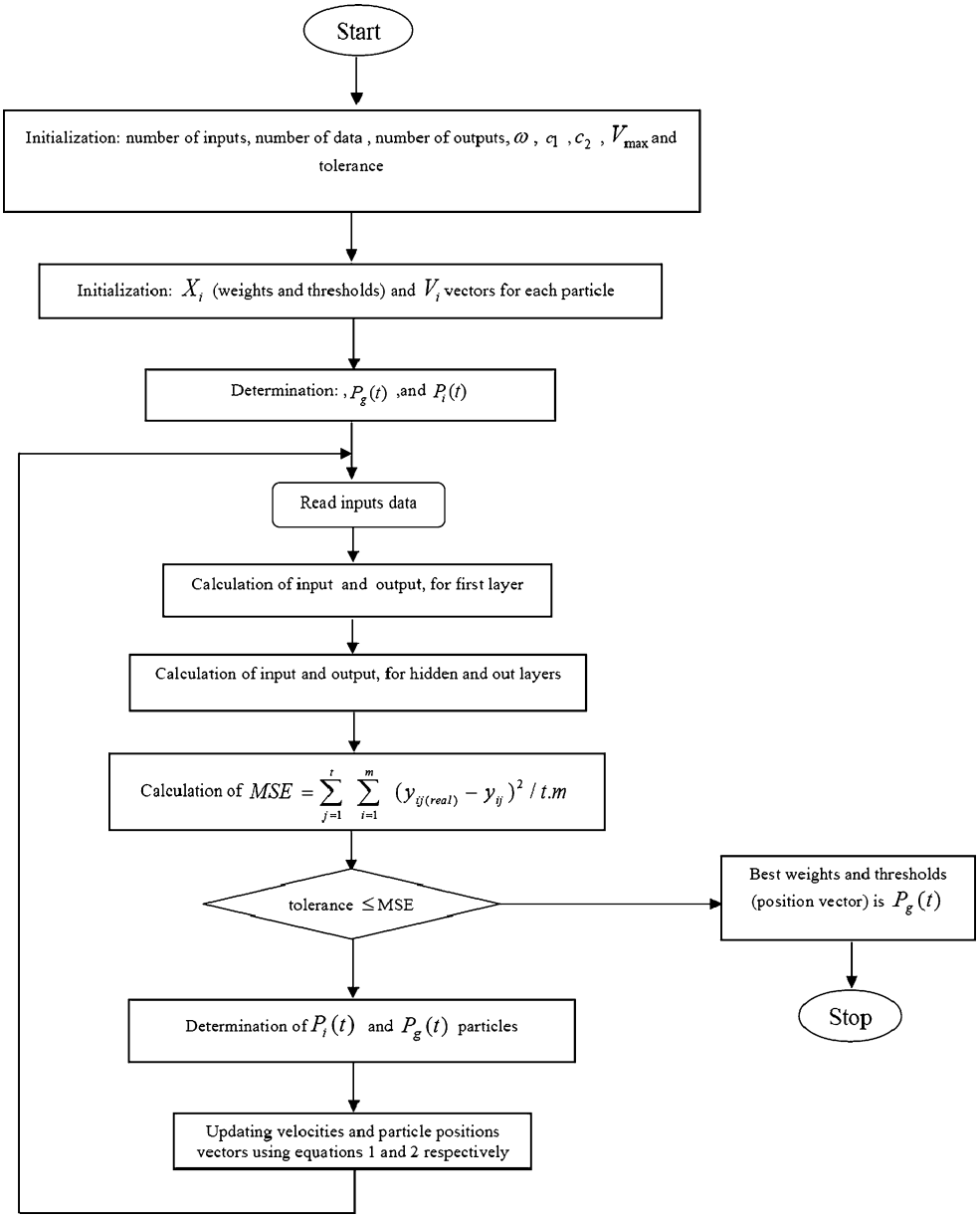

Fig. 1 Flow chart of the proposed modeling methodology using PSONN

As a result of nylon-6/nanoclay composite properties and potential applications, there exists a strong need to understand the manufacturing processes, particularly the machining of these nanocomposite materials. An increase in the desire for personalized products has led to the need for the direct machining of polymers for personalized products. The production of personalized products depends heavily on the types of equipment being used, respective technologies, and the selection of various types of materials. The ability to machine soft materials such as polymers offers distinct advantages for producing personalized soft consumer products, using direct machining [6]. But the machining of polymers often presents challenges to engineers in terms of close

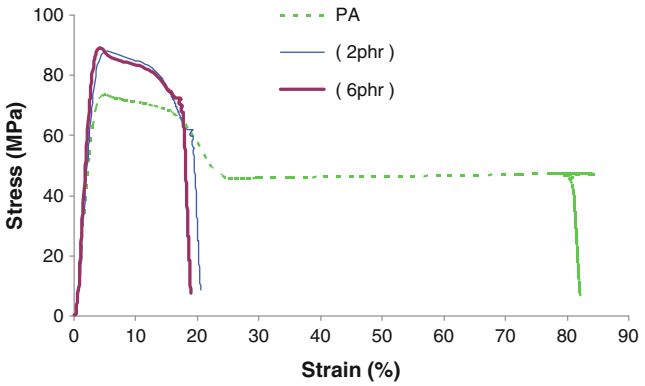

Fig. 2 Typical stress–strain curve for PA 6 and different nanocomposites

Table 1 Mechanical and thermal properties of PA-6 and different nanocomposites

Impact strength (KJ/m^2)	Tensile modulus (Gpa)	Tensile strength (Mpa)	NC content (phr)
40.027	2.797	76.44	0
37.4231	3.333	87.039	2
35.7949	3.548	88.492	6

tolerances, their unusual geometry, and softness, which means that it behaves differently as compared with conventional metal cutting [7].

The material properties significantly affect the success (or failure) of the machining operation. Surface roughness and specific cutting force are two important criteria used for evaluating the machinability of a composite material. These properties and other characteristics of the work are summarized in terms of its machinability, which indicates the relative ease to machine a given material using appropriate tooling and cutting parameters. Several criteria may be used to evaluate machinability, but the most important are tool life, cutting forces, and surface roughness [8]. The study of the dynamics of cutting forces and surface roughness is critical in any machining process for the proper planning and control of the machining operation and for the optimization of the cutting conditions aiming to reduce production costs and time. Cutting force analysis plays a vital role in studying the various characteristics of a machining process, for instance, the dynamic stability, positioning accuracy of the tool, and roughness of the machined surface [9].

Surface roughness on a nanocomposite material, as for other materials, is also contributed by tool geometry and material properties, cutting kinematics, and cutting conditions [10]. The measurement of surface roughness is used to determine the surface quality of the machined surfaces.

There is explicit information available on the machining of metals, whereas knowledge regarding the machining of polymers and their nanocomposites is limited. In recent years, there are few works on machining of polymers composites in milling and turning operations. Paulo Davim and Mata present an experimental study on the cutting process for polyamides PA 6 and PA 66-GF30 (reinforced with 30% glass fiber). In another work, Davim et al. studied the machinability of PA 66 with and without 30% glass fiber reinforcing, when precision turning at different feed rates and using four distinct tool materials [11, 12]. Dhokia et al., in an initial attempt, worked to extract information about the machining of soft materials with a focus on defining the optimum machining parameter for a machined polypropylene product. In another work, they presented a predictive model using a design of experiments strategy to obtain optimized machining parameters for a specific surface roughness in ball-end machining of polypropylene [6, 13].

Most of the time, it is very difficult to find the related analytical or empirical expressions and proper coefficients to calculate the optimal cutting conditions for the considered material and tool. Recently, analytical and empirical models have been developed by using neural network in order to calculate surface roughness for several materials [14, 15]. Also, the neural network model coupled with the genetic algorithm (GA) is proposed to determine the optimal machining for surface roughness [16, 17]. In recent years, a new evolutionary algorithm (EA) called particle swarm optimization (PSO) was developed. The PSO has fewer parameters and is easier to implement than the GA methods. The PSO has also shown a faster convergence rate than the other EAs for solving five optimization problems [18]. Successful applications of PSO to some optimization problems such as function minimization [19, 20] and artificial neural network design [21, 22], have demonstrated its potential.

In an initial work, this paper investigates the influence of the effects of nanoclay and cutting parameters on machinability of polyamide-6 (PA-6) nanocomposites in milling. To this end, the influence of cutting parameters (spindle speed and feed rate) on the cutting force and the surface roughness (R_a) of nano-

Fig. 3 Actual machining operation

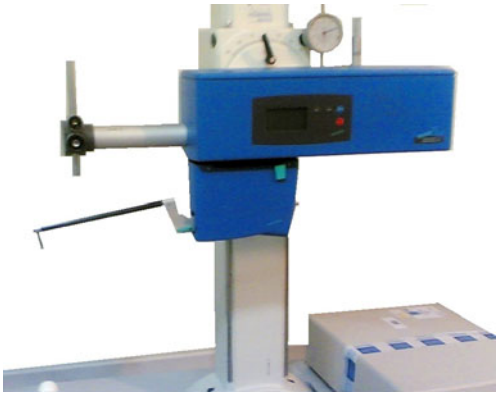

Fig. 4 Surface roughness measurement

composite materials using high speed steel (HSS) end mill are examined. Then cutting force and surface roughness are separately modeled by using particle swarm optimization-based neural network (PSONN). The capacity modeling of PSONN has been compared to that of the conventional neural network (NN) (backpropagation based on Levenberg–Marquardt algorithm).

The codes of PSONN are written in visual C++ language and optimal conventional neural network architecture is designed using MATLAB Neural Network Toolbox.

2 Particle swarm optimization-based neural network

Particle swarm optimization is a population-based stochastic optimization algorithm which has been proposed by Eberhart and Kennedy in 1995 [23]. It is considered to be capable to reduce the ill effect of the backpropagation (BP) algorithm of feedforward ANNs (e.g., very slow convergence speed in training, ease to get stuck in a local minimum, etc.), because it does not require gradient and differentiable information [18]. Also, it has proven to be a good competitor to the GA when it comes to optimization problems [19].

In PSO algorithm, each single solution is a "particle". All particles have fitness values, which are evaluated by the fitness function to be optimized, and have velocities, which direct the flying of the particles. The particles are flown through the problem space by following the current optimum particles. PSO is initialized with a group of random particles (solutions) and then searches for optimal by updating generations. In one iteration, each particle is updated by following two best values. The first one is the best solution (fitness) achieved so far (individual best position). Another best value tracked by the particle swarm optimizer, is the best value, obtained so far by any particle in the population (global best position); so, the velocity and position of the obtained optimum solution (particle) is updated during the iterative process. The stop criteria are reaching the maximum iteration number or satisfaction of the minimum error condition.

Although usually conventional PSO can find good solutions rapidly, it may be trapped in local minimum and fail to converge to the best position [18]. So, in recent years, some investigations have been done to deal with this problem [24, 25].

Suppose that the search space is n dimensional, the particles of the swarm can be represented by an n dimensional vector $X_i = [x_{i1}, x_{i2}, ..., x_{in}]^T \in S$, and the velocity of this particle can be represented by n dimensional vector $V_i = [v_{i1}, v_{i2}, ..., v_{in}]^T \in S$, where S is the searching space. The fitness of each particle can be evaluated according to the objective function of the optimization problem. $P_i(t) = [P_{i1}, P_{i2}, ..., P_{in}]$ is the last best position of the particle 'i', it is noted as its individual best position. The global best position is $P_g(t)$ and the new velocity of particle will be assigned according to the following equations:

$$V_i(t+1) = \omega.V_i(t) + c_1.r_1.(P_i(t) - X_i(t)) + c_2.r_2.\big(P_g(t) - X_i(t)\big) \quad (1)$$

Where c_1 and c_2 are acceleration parameters, ω represents the inertia weight which decreases linearly from 1 to near 0 while training, and r_1 and r_2 are random numbers

Fig. 5 Schema of measuring of the 3 orthogonal components of cutting force in the workpiece (F_x, F_y, and F_z)

Table 2 Levels of variables

Variables	Level 1	Level 2	Level 3
NC content (phr)	0	2	6
Spindle speed (rpm)	630	1,250	2,500
Feed rate (mm/tooth)	0.03	0.07	0.11

ranging between 0 and 1. The velocities of the particles on each dimension are clamped to a maximum velocity: V_{max}. The new position of the particle "*i*" is calculated by the following equation:

$$X_i(t+1) = X_i(t) + V_i(t+1) \quad (2)$$

Figure 1 illustrates the flowchart of the PSONN algorithm. As shown in this figure, the first step is initialization, *I*, c1, c2, V_{max}, and tolerance. These parameters have very important rules to promote the network's efficiently. After that, the first particle position vectors (**X**) and velocity vectors (**V**) were initialized randomly (between 0 and 1) for each particle. And two of them were considered as $P_g(t)$,and $P_i(t)$ (randomly). Then according to feed forward network inputs, outputs for layers and mean square error (MSE) were calculated. Also $P_g(t)$,and $P_i(t)$ were determined again. After that, according to Eqs. 1 and 2, particle velocities and particle positions were updated.

3 Experimental procedure

4 Material

The PA6 used in this work was B5 from BASF. The nanofiller was Nanofil®9 provided by Southern Clay Products which is organically modified montmorillonite with good adhesion to PA-6. PA-6 pellets and NC powder which remained at 90°Cfor 12 h and were mixed with a high speed mixer at dry conditions. Nanocomposites with 2 and 6 phr nanoclay were prepared by melt mixing using a lab scale corotating twin-screw extruder (ZSK25, *L*/*D*=40). The screw configuration used includes two high mixing zones using kneading elements and enhances dispersive and distributive mixing in the system and the extruder was equipped with a circular die. Then, dry extruded pellets were injection molded into standard (ASTM D 638) tensile bars using a 3-ton Engel injection molding machine. After molding, the specimens were sealed and placed in a vacuum desiccator for a minimum of 24 h prior to mechanical testing, under dry conditions. Figure 2 shows the effect of nanoclay content on the yield strength for the two different nanocomposite samples and pristine PA-6. The mechanical and thermal properties of PA-6 and different nanocomposites are indicated in Table 1.

4.1 Tool and machine tool

The experiments were performed in a Deckel Maho DMU 70 V vertical axis computer numerical control (CNC) milling machine with a maximum spindle speed of 3,150 rpm and 3,000 mm/min maximum feed rate. The machine had a 5.5 KW spindle motor. The actual machining operation is illustrated in Fig. 3. The CNC part programs are created by employing TopSolid CAD/CAM software on a personal computer, Intel Pentium IV at 3.2 GHz. The experiments have been carried out in nanocomposite plates with 3 mm of thickness, using a two flute HSS end mill, with 3 mm diameter. HSS end mill was manufactured according to standard HSS end mills [26].

4.2 Surface roughness measurement

Hommel Tester T8000 of Hommelwerke firm was used in the experimental work to measure surface roughness. The tools measure surface roughness with probes, measure, and control in appropriate length and circumferences. To do this, three small regions on the machined surface are determined for measurements. Measurements

Table 3 ANOVA for the cutting force (F_w)

Source	DF	Sum of square	Variance	*F*	*F* α=5%	*P*
Feed rate (mm/tooth)	2	2,212.34	1,106.17	156.09	3.3690	59.37
Spindle speed (rpm)	2	1,177.88	588.94	83.11	3.3690	31.61
NC content (phr)	2	194.34	97.17	13.71	3.3690	5.21
Error	20	141.73	7.09		1.9898	3.80
Total	26	3,726.29				100

Table 4 ANOVA for surface roughness (R_a)

Source	DF	Sum of square	Variance	F	F α=5%	P
Feed rate (mm/tooth)	2	98.233	49.177	122.40	3.3690	91.95
Spindle speed (rpm)	2	0.481	0.240	0.60	3.3690	0.45
NC content (phr)	2	0.087	0.044	0.11	3.3690	0.08
Error	20	8.025	0.401		1.9898	7.51
Total	26	106.827				100

in these regions are conducted and the average value is recorded as the R_a. In Fig. 4, the used surface roughness measurement tool is shown. The tracing velocity and the cut-off lengths were fixed at 0.5 mm/s and 2.5 mm, respectively.

4.3 Cutting force measurement

In order to measure cutting forces, the workpiece was mounted on a Kistler 9255B three-component piezoelectric dynamometer, which, in turn, was mounted onto the machine's table (see Fig. 5). Data acquisitions were made through piezoelectric dynamometer by interface RS-232 to load three Kistler 5011B amplifiers and to the PC using the appropriate software Dynoware Kistler®.

Single-pass, linear cuts were executed according to the factor levels of each repetition. The minimum, maximum, and mean values were also calculated. The maximum value of each component was selected as most representative. The value of cutting force (F_w) was determined according to the following equation:

$$F_w = \sqrt{F_x^2 + F_y^2 + F_z^2} \tag{3}$$

where F_x, F_y, and F_z are the three orthogonal components of cutting force in N.

4.4 Design of experiments

In this work, 27 samples based on full factorial design of the experiments employing three-level cutting parameters and three-level nanoclay content are given in Table 2. A constant depth of cut of 1 mm was used using HSS end mill.

5 Results and discussion

The results of milling tests allowed the evaluation of the PA-6/nanoclay nanocomposites, using HSS end mill. The machinability was evaluated by F_w and R_a.

5.1 Analysis of variance

The observed values of F_w and R_a were used to determine the significant factors influencing the machining process. The significant parameters influencing the cutting force and surface roughness were found using the analysis of variance (ANOVA) procedure. Tables 3 and 4 show the ANOVA for cutting force and surface roughness, respectively. From these calculations, it is inferred that the feed rate has more influence on surface roughness as compared to cutting force. Further, it is also inferred that nanoclay content has greater influence on cutting force as compared to surface roughness.

5.2 Influence of the cutting parameters on the F_w

In Figs. 6, 7, and 8, the evolution of the cutting forces F_w, can be seen with the feed rate for the different spindle speed for nanoclay content, of 0, 2, and 6 phr, respectively. From these figures, it can be realized that the F_w increases with feed rate and decreases with the spindle speed. As can be seen in Fig. 9, the slope of decreasing the forces recorded when milling the PA-6/nanoclay nanocomposites was considerably lower at high spindle speed. This fact may be related to the semiductile behavior of the PA-6 (Table 1),

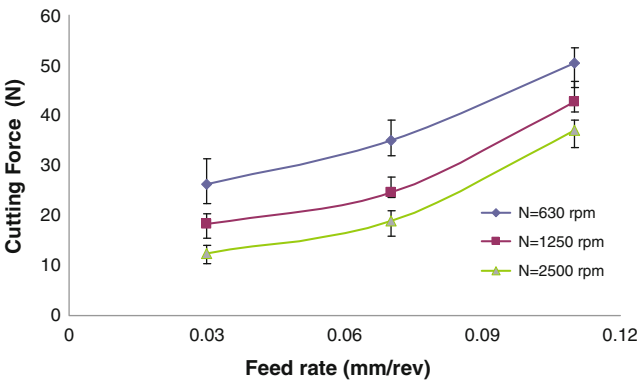

Fig. 6 Cutting force (F_w) as function of cutting parameters for pure PA-6

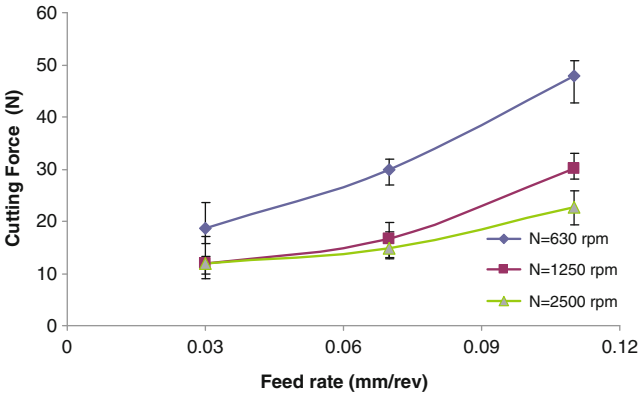

Fig. 7 Cutting force (F_w) as function of cutting parameters for PA-6, 2% nano clay

which would cause the softening of the work material on the rake face of the tool and adhesion of the work material on the rake face of the tool, which tends to slightly increase cutting forces. The burrs observed at the end of cutting at high spindle speed show evidence of melting of the material.

5.3 Effect of NC content on the cutting force F_w

Figure 10 shows the relationship between nanoclay content and cutting force F_w at different spindle speeds. As shown in this figure, the forces recorded when milling the PA-6/nanoclay nanocomposites were considerably lower compared to the pure polyamide. While it was seen in machining metals and polymer composites, that cutting forces increase with increasing the material hardness, the reverse effect was seen for nanocomposite samples, which can be attributed to the ductile behavior of the PA-6 nanocomposite.

For further elaboration, we use the proposed methodology which is based on the definition of the metal cutting process proposed by Astakhov [27]. According to this

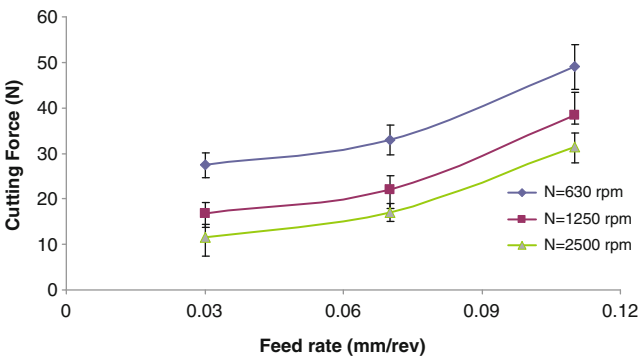

Fig. 8 Cutting force (F_w) as function of cutting parameters for PA-6, 6% nano clay

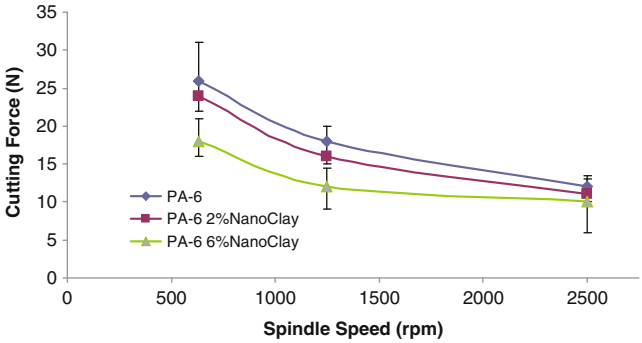

Fig. 9 Cutting force (F_w) as function of spindle speed for different material, feed rate 0.03 mm/rev

model, the power balance in the cutting system can be written as following equations:

$$P_c = F_c v = P_{\text{pd}} + P_{fR} + P_{fF} + P_{\text{ch}} \tag{4}$$

and the cutting force is calculated as:

$$F_w = \frac{P_{\text{pd}} + P_{fR} + P_{fF} + P_{\text{ch}}}{v} \tag{5}$$

where, P_{pd} is the power spent on the plastic deformation of the layer being removed, P_{fR} is the power spent at the tool–chip interface, P_{fF} is the power spent at the tool–workpiece interface, and P_{ch} is the power spent in the formation of new surfaces.

As Fig. 11 shows, the elastic modulus increases monotonically by increasing the NC content, and the elastic modulus of the sample with NC content of 6 phr shows an 26% increase compared to pristine PA-6.

Layered silicate has proved to contribute to properties improvement of the polymers in which they are dispersed.

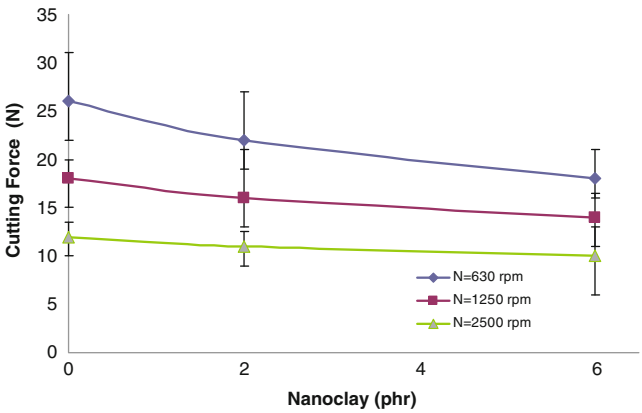

Fig. 10 Cutting force (F_w) as a function of nanoclay; feed rate= 0.03 mm/rev

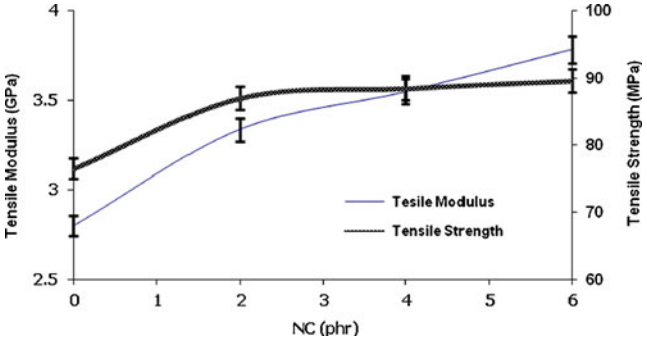

Fig. 11 Effect of nanoclay content on the tensile modulus and yield strength

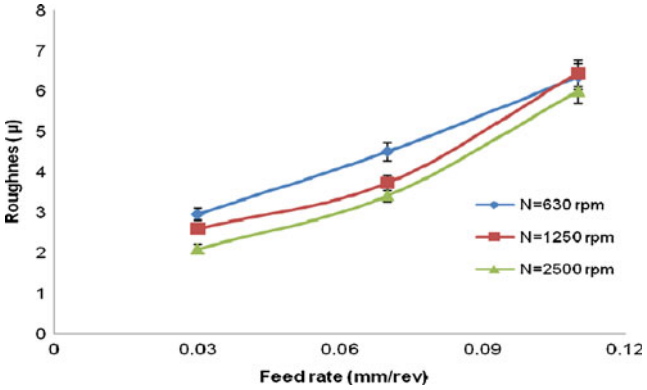

Fig. 13 Surface roughness (R_a) as function of cutting parameters for pure PA-6

Amongst those properties, unexpected enhancement in modulus of nanocomposites and fracture toughness decrement at low filler contents has drawn a lot of attention. The Young's modulus expressed as the stiffness of a material at the start of a tensile test has shown to be strongly improved when nanocomposites are formed.

The modulus of PA-6 nanocomposites is well known to be highly sensitive to the degree of exfoliation, since greater level of exfoliation lead to higher aspect ratio of filler particles which translates into better improvement of tensile modulus. The large increase in tensile modulus of nanocomposites with low NC content is an indication of the occurrence of exfoliation and intercalation and large interfacial area between the polymer and silicate layers [28]. The ability of dispersed silicate layers to increase the Young's modulus of PA-6 nanocomposites can be correlated to the average length of the layers, thus to the aspect ratio of the dispersed nanolayers. This increase of elastic modulus by increasing the NC content, results in decrease of plastic deformation of the layers of material being removed in cutting.

Power spent due to the friction at the tool–chip interface is directly proportional to the average shear stress at the tool–chip contact and the tool–chip contact length. As can be seen in Table 1, by increasing the NC content, the ultimate tensile strength of the different nanocomposite samples do not change effectively, but by increasing the NC content, the brittle behavior of the nanocomposite, increase monotonically. This brittle behavior decreases the tool–chip contact length and tends to decrease power spent due to friction at the tool–chip interface.

The power spent in the formation of new surfaces is proportional to the energy of fracture per shear plane. As it is illustrated in Fig. 12, increasing the NC content results in lower value for the fracture toughness parameter. It is believed that lower mobility of polymer chains due to intercalation in the gallery spacing of the rigid silicate layers results in lower toughness at higher NC contents. The reinforcing effect of NC is probably due to the incorporation of clay platelets in the PA-6 matrix. In addition, the decrease in elongation and break energy with NC content indicates that the resulting nanocomposites show brittle behavior. This decrease of fracture toughness parameter

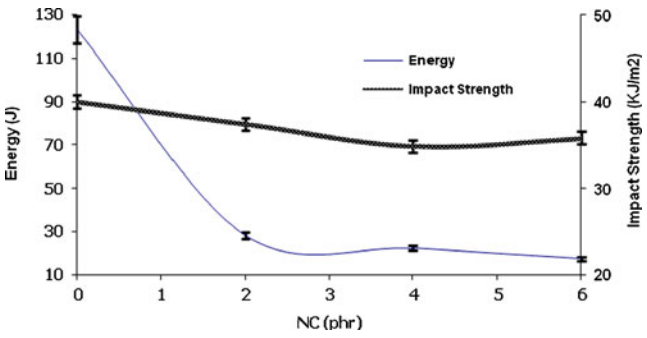

Fig. 12 Effect of nanoclay content on the energy at break

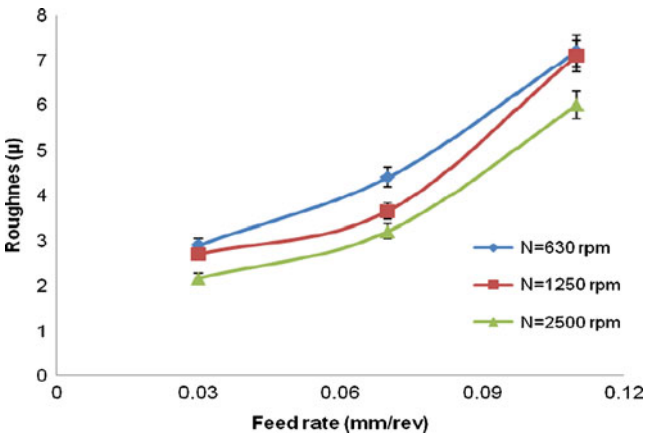

Fig. 14 Surface roughness (R_a) as function of cutting parameters for PA-6 2% nanoclay

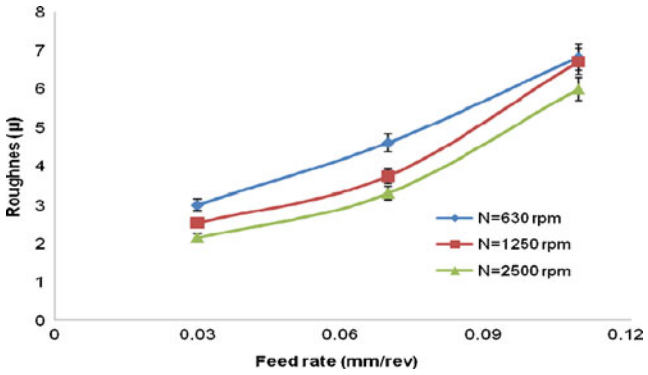

Fig. 15 Surface roughness (R_a) as function of cutting parameters for PA-6 6% nanoclay

by increasing the NC content, results in decrease of the power spent in the formation of new surfaces.

5.4 Influence of the cutting parameters on the surface roughness

In Figs. 13, 14, and 15, the evolution of the R_a, can be seen with the feed rate for different spindle speed of nanoclay content, of 0, 2, and 6 phr respectively. Figures 13, 14, and 15, show that the value of R_a increases when the feed rate does.

R_a decreases when the spindle speed increases. This fact may be related to ductile behavior of the PA-6 (Table 1), which would cause softening of the work material on the rake face of the tool and decrease shear stress of the material which results in easier cutting and better surface finish. So with a higher spindle speed and a lower feed rate, it is possible to obtain a better surface finish.

5.5 The effect of NC content on surface roughness

In Fig. 16, the evolution of the surface roughness R_a can be seen with nanoclay contents at different spindle speeds. It can be seen that nanoclay content does not have considerable influence on surface roughness. This may be related to the low shear stress of the PA-6 and its nanocomposites. However, shear stress of nanocomposites is lower than pure PA-6 but they are very low versus the HSS tool that can affect surface cutting.

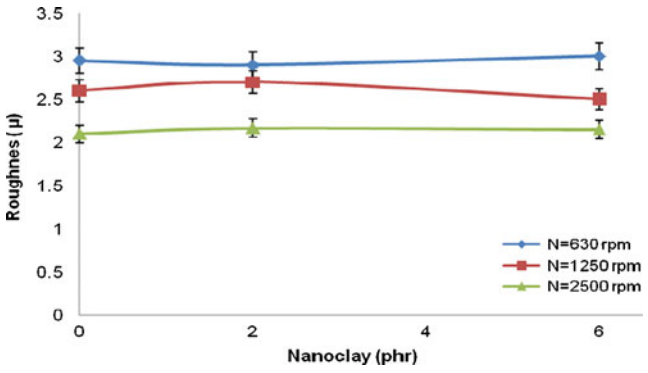

Fig. 16 Surface roughness (R_a) as a function of nanoclay, feed rate= 0.03 mm/rev

6 Modeling

6.1 Surface roughness modeling

The training subset includes 24 groups or 90% of the experimental data and the testing subset includes three groups or 10% of the data (not used in training) which were selected randomly out of each group in all parts. In order to find out the best possible network for surface roughness, different architectures (not presented in the paper) and nine combinations of training–testing sets based on cross-validation method (by using PSONN) were tested. In cross-validation algorithm, the dataset is divided into a number of equal sized divisions. For each of these, one division is used for the test data, and the others are used for training and selection. This allows the training algorithm to use virtually the entire dataset for training. In this study 27 datasets are divided to nine equal groups (three data in each group) and each group was used as test data and remained groups (24 data) were used for training. Table 5 shows the results of cross-validation in surface roughness modeling.

Finally, the PSONN model with 3-7-1 architecture was selected for surface roughness modeling. Moreover, the inertia weight (ω) linearly decreases from 0.9 to 0.02, c1 and c2 are equal to 2.1 and the number of particles in each subspace is 35. The maximum and minimum velocity values are 6 and −6, respectively (cf.

Table 5 Results of cross-validation in surface roughness modeling

Test numbers	Training (error)	Testing error
7-11-27	0.031	0.032
4-10-22	0.029	0.036
9-12-23	0.032	0.034
8-14-21	0.026	0.037
2-16-25	0.021	0.027
3-17-20	0.038	0.035
5-13-24	0.032	0.028
6-19-15	0.027	0.031
1-18-26	0.026	0.033

Table 6 Comparison of neural networks predictions with experimental measurement (R_a) for the test set

Test number	Spindle speed (rpm)	Feed rate (mm/tooth)	NC content (phr)	Experiment R_a (μm)	BP (NN)	Error (%)	PSONN	Error (%)
2	630	0.07	0	4.51	3.484	14.40	4.231	5.90
16	2,500	0.03	2	2.17	1.981	8.70	2.087	3.82
25	2,500	0.03	6	2.15	2.195	2.09	2.113	1.72

Eqs. 1 and 2). The training and checking MSE are obtained as 0.021 and 0.0269, respectively, after 277 iterations. The Bayesian regularization backpropagation based on Levenberg–Marquardt algorithm selected for training the backpropagation-based NN. It minimizes a combination of squared errors and weights, and then determines the correct combination so as to produce a network that generalizes well. The backpropagation-based NN model with 3-5-1 architecture is selected. MSE for training and testing data are obtained as 0.047 and 0.0325, respectively, after 322 epochs. Table 6 shows the comparison of neural networks predictions with experimental measurement (R_a) for the test set during testing the PSONN and backpropagation-based NN. In particular, PSONN has demonstrated improvement in training average error as compared to the backpropagation algorithm.

The results demonstrated that PSO algorithm has better performance and faster convergence speed than BP algorithm. The reason is that in PSONN a local gradient descending method is used to search around global optimum. Beside in comparison with BP, PSONN has some attractive characteristics. It retains previous useful information and encourages constructive cooperation and information sharing between particles, which enhance the search for a global optimal solution.

Table 7 Results of cross-validation in cutting forces modeling

Test numbers	Training (error)	Testing error
3-18-22	0.081	0.317
4-14-20	0.075	0.276
8-15-19	0.102	0.327
1-16-27	0.085	0.305
9-12-24	0.117	0.298
7-11-25	0.085	0.253
6-17-21	0.069	0.245
2-10-27	0.067	0.321
5-13-23	0.075	0.279

6.2 Cutting force modeling

For cutting force modeling, the training subset includes 24 groups of the experimental data and the testing subset includes three of the data (not used in training) which were selected randomly out of group in all parts. In order to find out the best possible network for cutting force modeling, different architectures (not presented in the paper) and nine combinations of training–testing sets based on cross-validation method (by using PSONN) were tested. Table 7 shows the results of cross-validation in cutting force modeling.

Finally, the PSONN model with 3-4-3-1 architecture selected, the inertia weight, is linearly decreases from 0.9 to 0.01, c1 and c2 are equal to 2 and the number of particles in each subspace is 30. The maximum and minimum velocity values are 7 and −7, respectively (cf. Eqs. 1 and 2). The training and checking MSE are obtained as 0.069 and 0.245, respectively, after 350 iterations. The Bayesian regularization backpropagation based on Levenberg–Marquardt algorithm was selected for training the backpropagation-based NN. It minimizes a combination of squared errors and weights, and then determines the correct combination so as to produce a network that generalizes well. The backpropagation-based NN model with 3-4-1 architecture is selected. The MSE for training and testing data are obtained as 0.953 and 2.54, respectively, after 519 epochs. Table 8 shows the comparison of neural networks predictions with experimental measurement (F_w) for the test set during testing the PSONN and backpropagation-based NN. In particular, PSONN has demonstrated improvement in training average error as compared to the backpropagation algorithm.

In neural network concept, overfitting likely occurs when trying to determine more fitting parameters than the number of data pairs. Sometimes overfitting has definitely occurred when trying to determine more fitting parameters than the number of data pairs. As can be seen in the errors of testing and training in cutting forces modeling an overfitting is obvious for both models while it cannot be seen in the results of surface roughness modeling. The reason is that in cutting force modeling case, the relation-

Table 8 Comparison of neural networks predictions with experimental measurement (F_w) for test set

Test number	Spindle speed (rpm)	Feed rate (mm/tooth)	NC content (phr)	Experiment F_w (*N*)	BP (NN)	Error (%)	PSONN	Error (%)
6	1,250	0.11	0	42.7	43.87	2.02	42.24	1.74
17	2,500	0.07	2	17.1	15.78	7.13	17.32	1.88
21	630	0.11	6	47.9	45.47	4.85	48.04	0.50

ship between the output and inputs in a neural network is more complex and nonlinear than the surface roughness, but result shows that PSONN could successfully adjust itself with the complex data and had less overfitting than backpropagation algorithm.

7 Conclusions

Based on the experimental results presented, the following conclusions can be drawn from milling PA-6/NC nanocomposites using HSS end mills:

- Cutting force increases when the feed rate increases and cutting force increases when the spindle speed decreases, i.e., at a higher spindle speed and a lower feed rate, cutting force is lower.
- Pure PA-6 has a higher cutting force in comparison with PA-6 nanocomposites. The slope of decreasing forces is being decreased with increasing the nanoclay content
- Surface roughness increases when the feed rate increases and surface roughness decreases when the spindle speed increases; with a higher spindle speed and a lower feed rate it is possible to obtain a better surface finish.
- The addition of nanoclay to the PA-6 significantly decreases the cutting forces, but does not have any considerable effect on surface roughness.
- Feed rate is the cutting parameter that presents the highest statistical and physical influence on surface roughness and on cutting force.

This study has also discussed the application of PSO-based NN, for determining modeling of cutting parameters leading to prediction cutting force and surface roughness values in the milling of PA-6/NC nanocomposites. The results have been compared to the conventional neural network algorithms and it demonstrated that PSO algorithm had better performance and faster convergence speed than BP algorithm. Beside in comparison with BP, PSONN retains previous useful information and encourages constructive cooperation and information sharing between particles, which enhance the search for a global optimal solution. The results showed that the PSONN can be used reliably, successfully and very accurately for the modeling of milling of PA-6/NC nanocomposites operation.

Conflict of interest The authors declare that they have no conflict of interest.

References

1. Giannelis EP (1996) Polymer layered silicate nanocomposites. Adv Mater 8:29–35
2. Biswas M, Ray SS (2001) Recent progress in synthesis and evaluation of polymer–montmorillonite nanocomposites. Adv Polym Sci 155:167–221
3. Alexandre M, Dubois P (2000) Polymer-layered silicate nanocomposites: preparation, properties and uses of a new class of materials. Mater Sci Eng 28:1–63
4. Kojima Y, Usiki A, Kawasumi M, Okada A, Fukushima Y, Karauchi T, Kamigaito O (1993) Synthesis of nylon-6–clay hybrid. J Mater Res 8:1179–1184
5. Kato M, Usiki A (2000) In polymer–clay nanocomposites. Wiley, New York
6. Dhokia VG, Kumar S, Vichare P, Newman ST, Allen RD (2007) Surface roughness prediction model for CNC machining of polypropylene. Proc IMechE Part B: J Eng Manuf 222:137–153
7. Fang FZ, Liu YC (2004) On minimum exit-burr in micro cutting. J Micromech Microeng 4:984–988
8. Mata F, Reis P, Davim JP (2006) Physical cutting model of polyamide composites (PA66 GF30). Mater Sci Forum 514–516:643–647
9. Wang W, Kweon SH, Yang SH (2005) A study on roughness of the micro-end-milled surface produced by a miniatured machine tool. J Mater Process Technol 162–163:702–708
10. Dagnal MA (1986) Exploring surface texture. Rank Taylor Hobson, Leicester
11. Davim JP, Mata F (2007) A comparative evaluation of the turning of reinforced and unreinforced polyamide. Int J Adv Manuf Technol 33:911–914
12. Davim JP, Silva LR, Festas A, Abrao AM (2009) Machinability study on precision turning of PA66 polyamide with and without glass fiber reinforcing. Mater Des 30:228–234
13. Dhokia GV, Kumar S, Vichare P, Newman TS (2008) An intelligent approach for the prediction of surface roughness in ball-end machining of polypropylene. Robot Comput-Integr Manuf 24:835–842

14. Krimpenis A, Fousekis A (2005) Assessment of sculptured surface milling strategies using design of experiments. Int J Adv Manuf Technol 25:444–453
15. Omar OEEK, El-Wardany T, Ng E, Elbestawi MA (2007) An improved cutting force and surface topography prediction model in end milling surface roughness in high-speed flat end milling. Mach Tools Mf J 47:1263–1275
16. Tansela IN, Ozcelikb B, Baoa WY, Chena P, Rincona D, Yanga SY, Yenilmezc A (2006) Selection of optimal cutting conditions by using GONNS. Mach Tools Mf J 46:26–35
17. Razfar MR, Zanjani Zadeh MR (2009) Optimum damage and surface roughness prediction in end milling glass fiber-reinforced plastics, using neural network and genetic algorithm. Proc IMechE Part B: J Eng Manuf 223:653–664
18. Yu Y, Wang S, Xi L (2008) Evolving artificial neural networks using an improved PSO and DPSO. Neurocomputing 71:1054–1060
19. Ratnaweera A, Saman K, Watson HC (2004) Self-organizing hierarchical particle swarm optimizer with time-varying acceleration coefficients. IEEE Trans Evol Comput 8(3):240–255
20. Guo YW, Mileham AR, Owen GW, Maropoulos PG, Li WD (2008) Operation sequencing optimazation for five-axis prismatic parts using a particle swarm optimization approach. Proc IMechE Part B: J Eng Manuf 223:485–497
21. Zhang JR, Zhang J, Lok TM, Lyu MR (2007) A hybrid particle swarm optimization–back-propagation algorithm for feedforward neural network training. Appl Math Comput 185:1026–1037
22. Kiranyaz V, Ince T, Yildirim A, Gabbouj M (2009) Evolutionary artificial neural networks by multi-dimensional particle swarm optimization. Neural Netw 22:1448–1462
23. Eberhart RC, Kennedy J (1995) A new optimizer using particle swarm theory, In Proceedings of the Sixth International Symposium on Micro machine and human science, 4–6 Oct. 1995, pp. 39–43 (IEEE Press, Piscataway, NJ). Nagoya, Japan.
24. Coelho LS (2009) An efficient particle swarm approach for mixed-integer programming in reliability-redundancy optimization applications. Reliab Eng Syst Saf 94(4):830–837
25. Jiang Y, Hu T, Huang CC, Wu X (2007) An improved particle swarm optimization algorithm. Appl Math Comput 193(1):231–239
26. SECO Milling 1 (2007) Catalogue & Technical Guide. SECO Tools AB, 737 82 Fagersta, Sweden
27. Astakhov VP (1998) Metal cutting mechanics. CRC, Boca Raton, USA
28. Moghri M, Garmabi H (2008) Investigation of effect of formulation and processing parameters on properties of PA 6 nanocomposites using taguchi method. Intern Polymer processing XXIII 5:430–438